The Plant Cell, Vol. 25: 4512–4524, November 2013, www.plantcell.org

Comparing the Calcium Binding Abilities of Two Soybean Calmodulins: Towards Understanding the Divergent Nature of Plant Calmodulins[W]

Jessica L. Gifford, Mostafa Jamshidiha, Jeffrey Mo, Hiroaki Ishida, and Hans J. Vogel[1]

Biochemistry Research Group, Department of Biological Sciences, University of Calgary T2N 1N4, Calgary, Alberta, Canada

ORCID ID: 0000-0002-2784-8517 (J.L.G.).

The discovery that plants contain multiple calmodulin (CaM) isoforms of variable sequence identity to animal CaM suggested an additional level of sophistication in the intracellular role of calcium regulation in plants. Past research has focused on the ability of conserved or divergent plant CaM isoforms to activate both mammalian and plant protein targets. At present, however, not much is known about how these isoforms respond to the signal of an increased cytosolic calcium concentration. Here, using isothermal titration calorimetry and NMR spectroscopy, we investigated the calcium binding properties of a conserved (CaM1) and a divergent (CaM4) CaM isoform from soybean (*Glycine max*). Both isoforms bind calcium with a semisequential pathway that favors the calcium binding EF-hands of the C-terminal lobe over those of the N-terminal lobe. From the measured dissociation constants, CaM4 binds calcium with a threefold greater affinity than CaM1 ($K_{d,Ca,mean}$ of 5.0 versus 14.9 μM) but has a significantly reduced selectivity against the chemically similar magnesium cation that binds preferentially to EF-hand I of both isoforms. The implications of a potential magnesium/calcium competition on the activation of CaM1 and CaM4 are discussed in context with their ability to respond to stimulus-specific calcium signatures and their known physiological roles.

INTRODUCTION

Ca^{2+} signaling systems are core regulators of the physiological and cellular processes of all eukaryotic organisms. In plants, a rapid and transient increase in the cytosolic and nuclear concentration of Ca^{2+} is observed in response to both abiotic (light, cold, heat, touch, wounding, drought, and oxidative stress) and biotic (phytohormones, pathogens, and symbiants) factors, triggering a myriad of cellular processes through which these organisms adapt to their environment (Reddy et al., 2011; Batistič and Kudla, 2012). Analogous to other eukaryotes, this Ca^{2+} signal is intercepted via high-affinity Ca^{2+} binding proteins that regulate, in a Ca^{2+}-dependent manner, the activity of their downstream targets. A major sensor of this Ca^{2+} signal in plant cells is the ubiquitous eukaryotic Ca^{2+} binding protein calmodulin (CaM) and the related CaM-like (CML) proteins (McCormack et al., 2005). Small, bilobal, and composed predominantly of α-helices, CaM contains two helix-loop-helix EF-hand Ca^{2+} binding motifs in each of its two globular domains (Figure 1A) (Gifford et al., 2007; Ishida et al., 2008). Upon binding Ca^{2+}, each lobe of CaM undergoes a closed to open conformational change through which the side chains of buried hydrophobic amino acid residues, particularly Met residues, are exposed (Yamniuk and Vogel, 2005; Yamniuk et al., 2009; Gifford et al., 2011). This creates two hydrophobic pockets that drive target binding.

Unlike animal cells, which have a single isoform of CaM encoded by three separate genes (Fischer et al., 1988), plants contain multiple CaM genes encoding several CaM isoforms with minor amino acid differences (Lee et al., 1995; Cho et al., 1998; Choi et al., 2002). These CaMs have varying degrees of sequence identity/similarity to the well-studied mammalian CaM (m-CaM) and represent conserved as well as more divergent CaMs. In addition to differing expression patterns that are modulated by developmental or environmental signals (Lee et al., 1995; Heo et al., 1999), in a number of studied plants, the various CaM isoforms selectively activate or inhibit CaM-dependent enzymes by virtue of a reciprocal target activation ability, and competition exists between the CaM isoforms for the CaM binding target proteins (Cho et al., 1998; Lee et al., 1999, 2000). In soybean (*Glycine max*), five known CaM genes encode four isoforms. Soybean CaM genes 1/3 and 2 (s-*CaM1/3* and s-*CaM2*) encode CaMs very similar in sequence to the conserved plant CaMs identified in alfalfa (*Medicago sativa*), barley (*Hordeum vulgare*), and *Arabidopsis thaliana*, as well as to that found in mammals (90 identical to m-CaM) (Figure 1B). In contrast, s-*CaM4* and s-*CaM5* encode more novel CaMs (77 and 75% identical to m-CaM, respectively, both 79% identical to s-CaM1); s-CaM4 differs from s-CaM1 by 32 out of 149 amino acids with 15 of the substitutions being nonconserved exchanges. Structural studies on the conserved s-CaM1 and divergent s-CaM4 indicate that the two proteins adopt a highly similar protein fold in the Ca^{2+}-bound state (Figure 1A) (Ishida et al., 2008), supporting mutational and biophysical experiments that point to the different activation abilities of the two isoforms as being due to very minor structural and chemical differences introduced by amino acid substitutions in the sequences of each protein (Kondo et al., 1999; Van Lierop et al., 2002; Yamniuk and Vogel, 2005). The sensitivity of CaM target proteins to the primary sequence of CaM underscores the potential for a sophisticated regulatory network given the diversity of CaMs and CaM binding proteins found in plants (Bouché et al., 2005).

An additional level of flexibility could be introduced into this signaling system by the different binding affinities of the various

[1] Address correspondence to vogel@ucalgary.ca.
The author responsible for distribution of materials integral to the findings presented in this article in accordance with the policy described in the Instructions for Authors (www.plantcell.org) is: Hans J. Vogel (vogel@ucalgary.ca).
[W] Online version contains Web-only data.
www.plantcell.org/cgi/doi/10.1105/tpc.113.113183

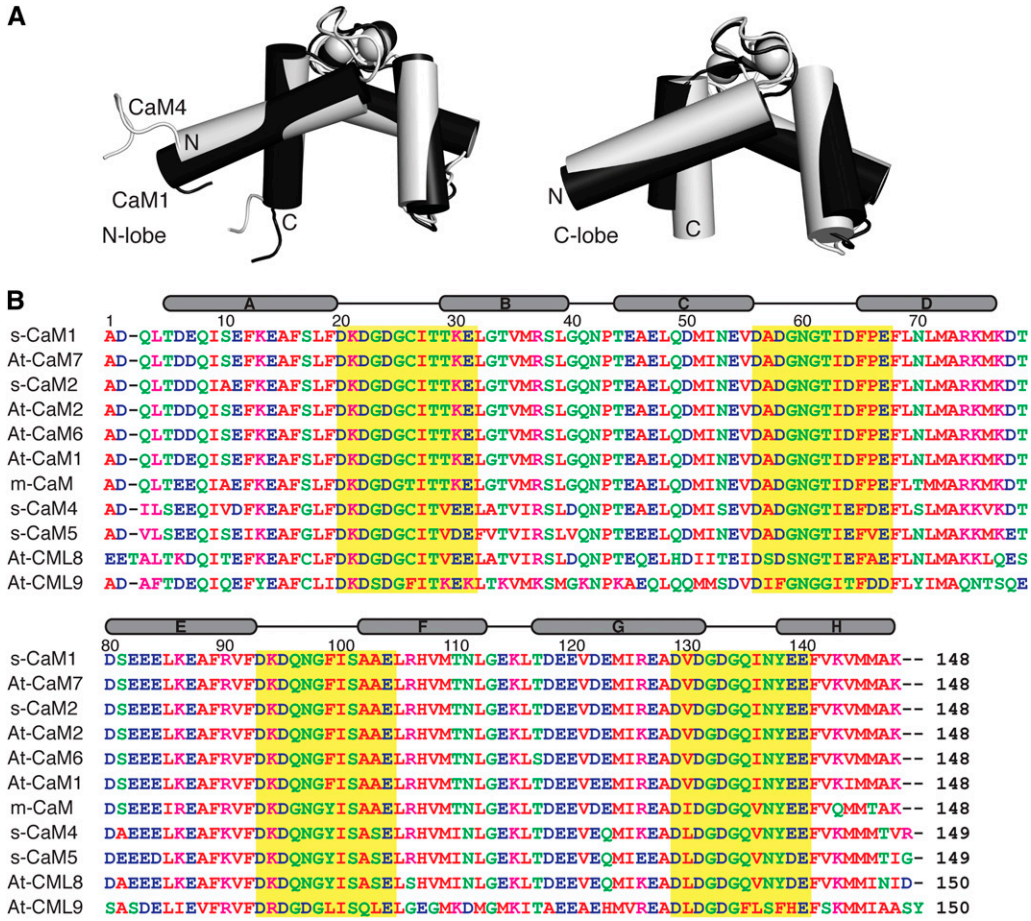

Figure 1. Sequence Comparison and Ca^{2+}-Bound Conformation of Soybean CaM1 and CaM4.

(A) Main-chain overlay of the N- and C-terminal lobes of Ca^{2+}-CaM1 (black) and Ca^{2+}-CaM4 (light gray) structures (Protein Data Bank codes: s-CaM1-N [2RO8], s-CaM1-C [2RO9], s-CaM4-N [2ROA], and s-CaM4-C [2ROB]). The structures overlay with a main-chain root mean squared deviation of 0.88 and 1.50 Å, respectively.

(B) Sequence alignment of conserved (s-CaM1/2, At-CaM1/2/6/7, and m-CaM) and divergent (s-CaM4/5) CaMs and select CMLs (At-CML8/9). The Ca^{2+} binding EF-loop is highlighted by a yellow box. The secondary structural elements are indicated above. The sequence conservation to s-CaM1 for each is as follows: At-CaM7 (0.99), s-CaM2 (0.98), At-CaM2 (0.98), At-CaM6 (0.98), At-CaM1 (0.97), m-CaM (0.90), s-CaM4 (0.79), s-CaM5 (0.79), At-CML8 (0.71), and At-CML9 (0.51).

CaM isoforms for Ca^{2+}, as this would modulate their ability to activate targets and hence create subsets of CaMs conditioned to decode particular Ca^{2+} signals. Here, we used biophysical techniques to investigate the Ca^{2+} binding properties of soybean CaM1 and CaM4 as well as the influence of the chemically similar magnesium cation (Mg^{2+}) on the abilities of these proteins to bind Ca^{2+}. We interpreted the observed Ca^{2+} binding abilities in the context of the specific physiological roles of these two CaM isoforms.

RESULTS AND DISCUSSION

Ca^{2+} Binds CaM1 and CaM4 through a Semisequential Binding Pathway Favoring the C-Terminal EF-Hands

Analogous to other helix-loop-helix EF-hand Ca^{2+} binding proteins, the apo- and Ca^{2+}-bound states of soybean CaM1 and CaM4 exist in distinct structural conformations (see Supplemental Figure 1 online). Readily observed in NMR spectra, the differences in conformation can be exploited to understand the binding pathway of the Ca^{2+} ions. Ca^{2+} titration of apo-CaM1 or apo-CaM4 was performed and monitored through rapidly acquired ^{1}H-^{15}N shift correlation experiments. In NMR spectroscopy, the spectra produced by the ^{1}H-^{15}N shift correlation class of experiments (including the [^{15}N-^{1}H]-HSQC [for heteronuclear single quantum coherence] or [^{15}N-^{1}H]-band-selective optimized-flip-angle short-transient heteronuclear multiple quantum coherence experiments used here) are very useful for studying protein–ligand interactions. In the [^{15}N-^{1}H]-HSQC spectra shown in Supplemental Figure 1 online, each dot represents the NMR signal (also known as a peak) from the amide (NH) group of each amino acid, and it is composed of the corresponding ^{1}H and ^{15}N chemical shift values. By comparing ^{1}H-^{15}N shift correlation spectra in the presence or absence of

a ligand, protein–ligand interactions can be monitored by the broadening and/or position shift of each peak in the ^{1}H-^{15}N shift correlation spectrum. For many EF-hand proteins, including CaM1 and CaM4, strengthening of intraloop hydrogen bonds causes the main chain NH groups of homologous Gly residues found at the sixth position of the four Ca^{2+} binding EF-loops (Gly_6: Gly-25, Gly-61, Gly-98, and Gly-134) to exhibit characteristic high (also described as downfield) ^{1}H chemical shift values in their Ca^{2+}-bound form (Figure 2A; see Supplemental Figure 1 online). The extent of this downfield shift places their corresponding NH peaks in the least crowded region of ^{1}H-^{15}N shift correlation spectra and enables them to act as indicators for the Ca^{2+}-bound state of a given EF-hand (Mukherjee et al., 2007; Aravind et al., 2008). Figure 2B presents the plots of normalized Ca^{2+}-bound Gly_6 NH peak intensity as a function of the Ca^{2+}:protein ratio for both CaM1 and CaM4. In the Ca^{2+} titration of both CaM isoforms, the Gly_6 signals for the C-terminal lobe begin to reach their Ca^{2+}-saturated chemical shift and intensity at Ca^{2+}:protein ratios much lower than those of the N-terminal sites. The NH peaks of the Ca^{2+}-bound C-terminal Gly_6 residues of CaM1 (Gly-98 and Gly-134) develop simultaneously around a Ca^{2+}:protein ratio of 2. By contrast, the peaks corresponding to the Ca^{2+}-bound N-terminal Gly_6 residues of this isoform (Gly-25 and Gly-61) develop together at a ratio of 4. The C-terminal Gly_6 NH peaks of CaM4 show up at their Ca^{2+}-saturated chemical shift almost together at a Ca^{2+}:protein ratio near 4, while those of the N-terminal EF-hands appear together at a ratio of 7:1. The preference of Ca^{2+} for the C-terminal EF-hands is an equivalent binding pattern to that seen with m-CaM and is termed a semi-sequential binding pathway (Linse et al., 1991).

This experiment reports on the occupancy (through signal intensity) of the Ca^{2+}-bound state of an EF-hand, not just the presence of a given Gly_6 NH peak at its Ca^{2+}-bound chemical shift. As a result, higher than stoichiometric Ca^{2+}:protein ratios were required to reach saturation. Furthermore, the outcomes of the titrations, a gradual increase in intensity of the C-terminal Gly_6 signals until saturation is observed versus the abrupt saturation of the N-terminal Gly_6 peaks at higher stoichiometric ratios, reflect the different exchange rates through which Ca^{2+} binds to the two lobes of CaM1 and CaM4. Ca^{2+} binds in fast to intermediate exchange to the N-terminal lobe of both isoforms and in slow exchange to the C-terminal lobe. The type of exchange accompanying ligand binding is directly proportional to the affinity of the interaction and the discrepancy in exchange rates suggests that, for both isoforms, Ca^{2+} binds more weakly to the EF-hands of the N-terminal domain than to those of the C-terminal domain.

Ca^{2+} Binds apo-CaM4 with Greater Affinity than apo-CaM1

The energetics of Ca^{2+} binding to CaM1 and CaM4 were studied through isothermal titration calorimetry (ITC), a technique used to determine the thermodynamic parameters of an interaction by measuring the heat taken in (endothermic) or evolved (exothermic) when a ligand is titrated into a macromolecule (protein, DNA, etc.). Experimental data for the binding of Ca^{2+} to both CaM1 and CaM4 are presented in Figure 3A. The binding of Ca^{2+} to the apo-state of either isoform is a multiphasic process as both CaM1 and CaM4 display exothermic and endothermic Ca^{2+} binding sites. Data were fitted with the stoichiometry of Ca^{2+} binding fixed to four, following a procedure used previously for m-CaM and similar EF-hand-containing Ca^{2+} binding proteins (Gilli et al., 1998; Mukherjee et al., 2007; Dagher et al., 2011). Although the presence of auxiliary Ca^{2+} binding sites has been proposed for CaM (Lafitte et al., 1995), they are too weak to be measured by ITC due to the high concentration of Ca^{2+} required for saturation (Gilli et al., 1998). The values for the obtained Ca^{2+} dissociation constants (K_{d1}, K_{d2}, K_{d3}, and K_{d4}), corresponding to the strength of the first, second, third, and fourth Ca^{2+} binding site on CaM1 or CaM4, are presented in Supplemental Table 1 online. As the binding of Ca^{2+} is an electrostatic interaction, these values reflect the pH, buffer, and ion strength of the solutions used but are comparable to those previously reported for both m-CaM and a synthetic hybrid of animal and plant CaM (Linse et al., 1991; Gilli et al., 1998). The NMR titration data presented above allow us to assign the dissociation constants to specific lobes of CaM1 and CaM4: K_{d1} and K_{d2} belong to the C-terminal lobe of both isoforms, whereas K_{d3} and K_{d4} match the N-terminal lobes. CaM4 has an overall Ca^{2+} affinity thrice that of CaM1 ($K_{d,Ca,mean}$ of 5.0 $\pm$ 0.8 μM versus 14.9 $\pm$ 1.8 μM, respectively) and binds Ca^{2+} with an 11 kJ mol^{-1} more favorable total Gibb's free energy change ($\Delta G_{1,2,3,4}$), an affinity increase spread equally over both domains of CaM4 (Table 1). Furthermore, Ca^{2+} binds to the C-terminal EF-hands of CaM1 and CaM4 with an $\sim$10 kJ mol^{-1} greater affinity than those found in the N-terminal lobe of each isoform. This value is analogous to the interlobe disparity seen with m-CaM (Linse et al., 1991) and explains the Ca^{2+} binding preference and difference in exchange behavior observed in our NMR titration experiments (Figure 2B).

Ca^{2+} Binds to CaM1 and CaM4 with Different Energetic Driving Factors

The thermodynamic parameters that accompany the binding of each Ca^{2+} ion to the sites in CaM1 or CaM4 are presented in Table 2. As evidenced by the relationships presented in Methods (Equations 1 and 2), the strength of Ca^{2+}'s interaction with each site is reflected in the magnitude of the decrease in free energy ($-\Delta G$) and dictated by the accompanying changes in the system's internal energy (also known as its enthalpy [ΔH]) and disorder (entropy [ΔS]). At a constant temperature ($T = 30$°C), a larger magnitude increase in ΔS or decrease in ΔH leads to higher affinity binding. The binding of Ca^{2+} to apo-CaM1 is an entropically driven process. The large, favorable value of the $-T\Delta S$ term dominates Ca^{2+} binding to all four EF-hands of CaM1 and compensates for the endothermic and, thus, unfavorable ΔH that accompanies Ca^{2+} binding to all but one EF-hand (Ca^{2+} binding site 3; Table 2). Ca^{2+} binding to CaM4 is impelled by a different set of energetic factors: Two of the sites are enthalpically favorable but entropically unfavorable (sites 1 and 4), while two are enthalpically unfavorable and entropically favorable (sites 2 and 3).

The protein–Ca^{2+} interaction is driven by two main thermodynamic mechanisms: (1) the desolvation of the cation as the water molecules that surround the cation are replaced by ligands from the protein (represented by $\Delta H_{binding}$ [ΔH_{bind}] and $\Delta S_{binding}$ [ΔS_{bind}]), and (2) the formation of favorable inter–amino acid residue contacts induced by a Ca^{2+}-dependent protein conformational change ($\Delta H_{conformation}$ [ΔH_{conf}] and $\Delta S_{conformation}$ [ΔS_{conf}]) (Gilli et al., 1998). The ΔH and ΔS determined using ITC are composed as

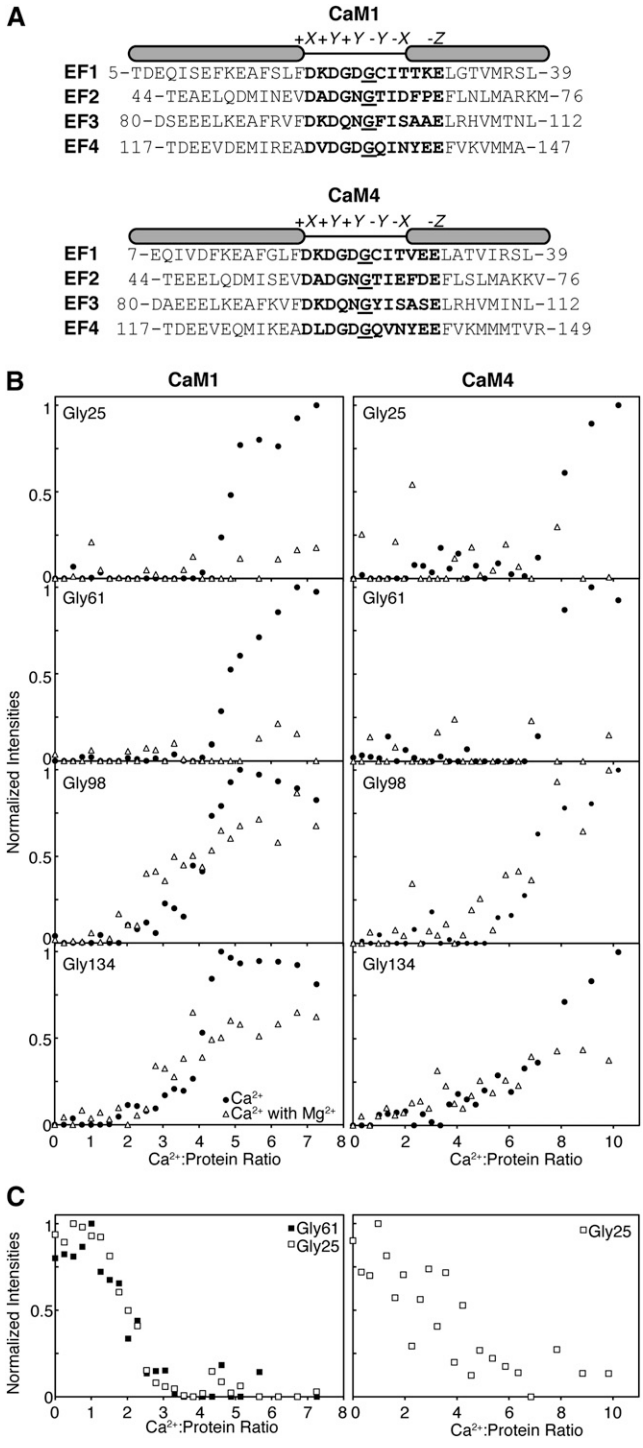

Figure 2. Ca^{2+} Binds to the C-Terminal Lobe of CaM1 or CaM4 before the N-Terminal Lobe in Both the Absence and Presence of Saturating Mg^{2+}.

(A) Alignment of the EF-hands of CaM1 and CaM4. The Ca^{2+}-coordinating EF-loops are highlighted (bold), including the Gly_6 used as a probe for cation binding (underlined). The positions of the amino acid ligands in Ca^{2+}'s pentagonal bipyramidal coordinating geometry are indicated above.

follows: $\Delta H = \Delta H_{bind} + \Delta H_{conf}$ and $\Delta S = \Delta S_{bind} + \Delta S_{conf}$. As the same ligand coordination geometry surrounds Ca^{2+} in water and in EF-hand Ca^{2+} binding loops, ΔH_{bind} can be approximated to zero and the measured ΔH corresponds primarily to ΔH_{conf} (Table 2) (Gilli et al., 1998; Yamniuk et al., 2004; Mukherjee et al., 2007). It is possible to discriminate between ΔS_{bind} and ΔS_{conf} if we measure the thermodynamic parameters of the protein–Ca^{2+} interaction under different experimental conditions (Figure 3B). For both isoforms, plots of ΔH versus ΔS are linear under all conditions tested. This indicates that there is a direct relationship between the enthalpy and entropy changes observed upon Ca^{2+} binding, suggesting a clear example of enthalpy-entropy compensation (Grunwald and Steel, 1995). Taking into account this relationship and that $\Delta H_{bind} = 0$, ΔS can then be defined as $\Delta S = k\Delta H + \Delta S_{intercept}$, where $\Delta S_{intercept}$ is equal to the entropy of Ca^{2+} desolvation (ΔS_{bind}). From our data, $\Delta S_{bind} = 90.6\ J\ K^{-1}\ mol^{-1}$, a value that agrees well with that obtained previously for a synthetic CaM (Gilli et al., 1998).

Using this information, we can identify the enthalpic and entropic contributions to the overall energetics of the Ca^{2+}–CaM1/4 interaction and glean information on the driving factors for the differences in Ca^{2+} affinity of the two isoforms. The binding of Ca^{2+} to three of the four EF-hands of CaM1 is accompanied by unfavorable changes in ΔH_{conf} (Table 2), a predictable outcome as the Ca^{2+}-dependent helical rearrangements lead to a loss of interhelical interactions. By subtracting ΔS_{bind} ($90.6\ J\ K^{-1}\ mol^{-1}$) from the entropy values listed in Table 2, we can calculate ΔS_{conf} for Ca^{2+} binding to CaM1. Values of 31 and 39 $J\ K^{-1}\ mol^{-1}$ for sites 1 and 2 suggest that Ca^{2+} binding to the C-terminal lobe of CaM1 induces a higher degree of conformational flexibility in the molecule. By contrast, the binding of this cation to the N-terminal EF-hands of CaM1 is accompanied by ΔS_{conf} values of -33 and $-12\ J\ K^{-1}\ mol^{-1}$ for sites 3 and 4, respectively. This loss in entropy can be attributed to a combination of increased molecular rigidity and the Ca^{2+}-induced exposure of hydrophobic target binding patches (see fluorescence spectroscopy data using 8-anilino-1-naphthalene sulfonic acid [ANS] below). Taken as a whole, our ITC data suggest the binding of Ca^{2+} to CaM1 is accompanied by energetically costly conformational changes and is therefore driven by the favorable desolvation of the Ca^{2+} cation (ΔS_{bind}).

The energetics of the interaction of Ca^{2+} with CaM4 are in contrast with those of CaM1. The magnitudes of the measured enthalpy and calculated entropy changes are much higher, and Ca^{2+} binding to the first EF-hand of the C-terminal lobe and last EF-hand of the N-terminal lobe is accompanied by favorable changes in enthalpy and overall unfavorable changes in entropy (Table 2; $\Delta S_{conf} = -331$ and $-585\ J\ K^{-1}\ mol^{-1}$ for sites 1 and 4, respectively). These thermodynamic values likely reflect the induced structure formation observed for this isoform upon binding

(B) Plots of normalized main-chain NH peak intensities observed in ^1H-^{15}N shift correlation spectra for CaM1 or CaM4 EF-loop Gly_6 residues as a function of the Ca^{2+}:protein ratio in the absence and presence of $MgCl_2$.

(C) Plots of normalized Gly_6 NH peak intensities present in Mg^{2+}-saturated ^1H-^{15}N shift correlation spectra as a function of Ca^{2+}:protein ratio.

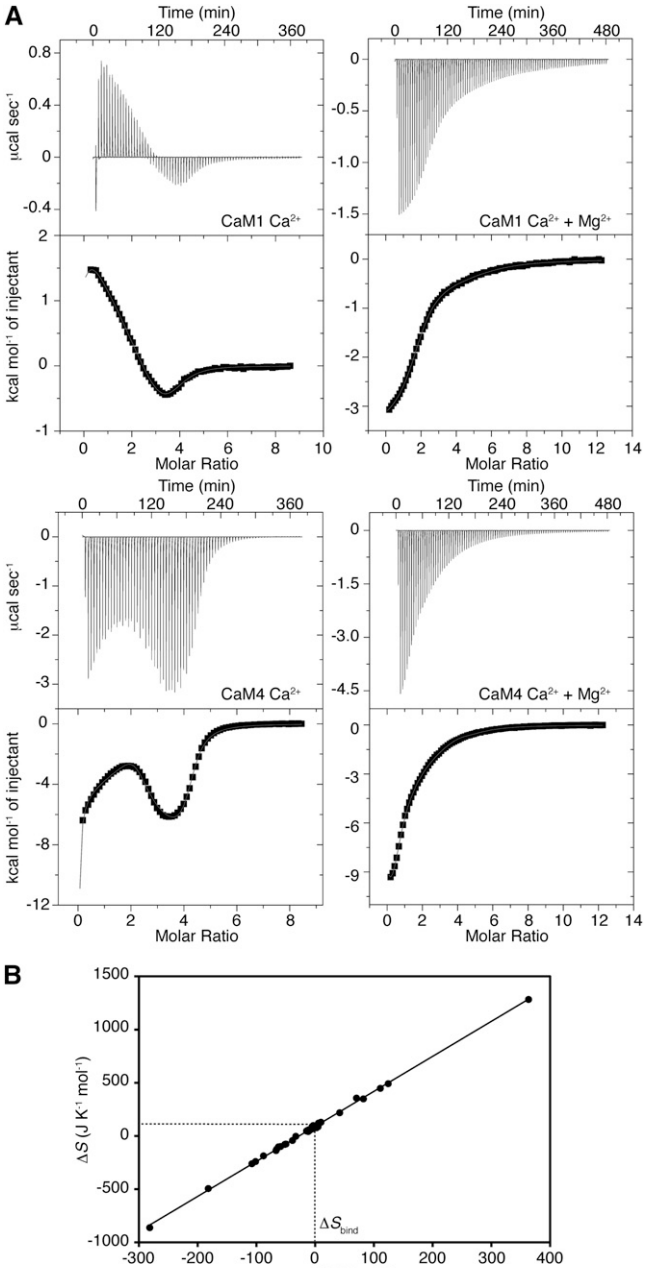

Figure 3. Calorimetric Titration of CaM1 or CaM4 with Ca^{2+} in the Presence and Absence of $MgCl_2$.

(A) Plots of kcal mol^{-1} of heat absorbed/released per injection of $CaCl_2$ as a function of Ca^{2+}:protein ratio in the absence and presence of 10 mM $MgCl_2$. The least-squares fit of the data to a four site sequential binding model is given by the solid line.

(B) Enthalpy-entropy relationship for Ca^{2+} binding to the four EF-hands of CaM1 and CaM4. The data points represent the ΔH and ΔS for each Ca^{2+} binding site measured in 0, 0.5, 2, 5, 10, or 30 mM $MgCl_2$. ΔS_{bind} for Ca^{2+} can be determined from the *y*-intercept of the line described by $\Delta S = k\Delta H + \Delta S_{intercept}$.

Ca^{2+} (see Supplemental Figure 1 online; Huang et al., 2010), a process accompanied by favorable changes in enthalpy due to electrostatic and hydrogen bond formation and a corresponding loss of flexibility and decrease in system entropy. The binding of Ca^{2+} to the partner EF-hands of these sites is enthalpically unfavorable and paired with an increase in conformational entropy (ΔS_{conf} = 266 and 401 J K^{-1} mol^{-1} for sites 2 and 3, respectively), likely reflecting the loss of interhelical contacts as the buried hydrophobic side chains are exposed. Altogether, these ITC data suggest that CaM4's increased Ca^{2+} affinity can be attributed to the structural instability of the apo-state of CaM4, and both energetically favorable conformational changes and favorable cation desolvation accompany Ca^{2+} binding to this isoform.

Mg^{2+} Binds to the EF-Loops of CaM1 and CaM4

Although the total Mg^{2+} content in a plant cell ranges from 15 to 25 mM, most Mg^{2+} cations are complexed with cellular components (phospholipids, phosphonucleotides, proteins, chlorophyll, etc.), and the free Mg^{2+} concentration is much lower, in the range of 0.4 to 0.5 mM (Waters, 2011). This concentration can rise to 1 mM or higher as a result of rapid expenditures of the Mg^{2+}-chelator ATP and drop in pH that occur when the plant is stressed (Igamberdiev and Kleczkowski, 2001, 2011). The comparable chemical properties of Mg^{2+} and Ca^{2+} (similar atomic size; preference for carboxyl, carbonyl, or hydroxyl protein ligands) lead to a complicated case of cation selectivity as Ca^{2+} binding proteins must discriminate against a 10^2- to 10^4-fold excess of the Mg^{2+} cation (Gifford et al., 2007; Gifford and Vogel, 2013). Like many other EF-hand proteins, both CaM1 and CaM4 bind Mg^{2+}, and ^1H-^{15}N shift correlation spectra indicate the Mg^{2+}-bound conformations of the two isoforms are both folded and distinct from the apo- or Ca^{2+}-bound structures (see Supplemental Figure 1 online; Huang et al., 2010).

Controversy has surrounded the location and number of Mg^{2+} binding sites in m-CaM, and Mg^{2+} has been proposed to act either as a direct competitor or as an allosteric regulator of Ca^{2+} binding to this CaM (Ohki et al., 1997; Gilli et al., 1998; Malmendal et al., 1999). The accepted model now considers Mg^{2+} to be a direct competitor of Ca^{2+} for the EF-hands of m-CaM, and NMR data, particularly the downfield shifted Gly_6 NH signals, point to the Mg^{2+} binding sites being located within the EF-loop structure. The ^1H-^{15}N shift correlation spectrum of Mg^{2+}-bound CaM1 or CaM4 show two downfield shifted Gly_6 residues for CaM1 and one downfield shifted Gly_6 residue for CaM4 (see Supplemental Figure 1 online). The assignment of these peaks in the Mg^{2+}-CaM1 NMR spectrum as belonging to residues Gly-25 and Gly-61 of EF-hands I and II, respectively, was determined by conventional triple resonance experiments. A previous NMR signal assignment of Mg^{2+}-CaM4 identifies the single downfield residue as Gly-25 of EF-hand I (Huang et al., 2010).

The relative strength of Mg^{2+}'s affinity for the EF-hands of both isoforms can be inferred from peak quality in ^1H-^{15}N shift correlation spectra and signal saturation observed in NMR Mg^{2+} titrations. Much like that seen previously with soybean CaM4 (Huang et al., 2010), only the N-terminal domain of Mg^{2+}-CaM1 gave rise to a near complete assignment of the NMR signals from the main chain atoms (85 and 92% for CaM1 and CaM4, respectively;

Table 1. Ca^{2+} Affinities and Free Energies of Binding for CaM1 or CaM4 in the Absence and Presence of Mg^{2+}

CaM	$K_{d,N,ave}$ (μM)[a]	$K_{d,C,ave}$ (μM)[b]	$K_{d,ave}$ (μM)[c]	ΔG_N (kJ mol^{-1})	ΔG_C (kJ mol^{-1})	$\Delta G_{1,2,3,4}$ (kJ mol^{-1})
s-CaM1	36.2 ± 7.4	6.2 ± 0.2	14.9 ± 1.8	−51.8 ± 1.1	−60.4 ± 0.1	−112.2 ± 1.2
+ 10 mM Mg^{2+}	107.8 ± 5.5	14.8 ± 0.6	39.8 ± 0.5	−46.1 ± 0.2	−56.1 ± 0.2	−102.1 ± 0.0
s-CaM4	13.0 ± 0.8	2.0 ± 0.5	5.0 ± 0.8	−56.9 ± 0.7	−66.3 ± 1.2	−123.3 ± 1.8
+ 10 mM Mg^{2+}	29.2 ± 6.6	34.1 ± 6.8	31.5 ± 6.7	−52.8 ± 0.9	−52.0 ± 1.0	−104.9 ± 1.9

From our NMR data, sites 1 and 2 can be assigned to the C-terminal lobe and sites 3 and 4 to the N-terminal lobe.
[a] $K_{d,N,ave} = (K_3K_4)^{-1/2}$.
[b] $K_{d,C,ave} = (K_1K_2)^{-1/2}$.
[c] $K_{d,ave} = (K_1K_2K_3K_4)^{-1/4}$.

compared with total assignments of 76 and 69%; see Supplemental Figure 2A online). By contrast, the C-terminal domains of both isoforms have a number of missing signals attributable to peak broadening. The majority of the missing signals are centered in or near EF-loops III and IV, suggesting that the weak interaction of Mg^{2+} with these C-terminal EF-hands is causing localized fluctuations in the protein conformation. Alternatively, the conformational stability observed for the N-terminal lobe of both proteins points to Mg^{2+} binding preferentially to EF-hands I and II. Of these two EF-hands, signal saturation at lower Mg^{2+} concentrations in an NMR titration experiment points to EF-hand I of apo-CaM1 as being the higher affinity Mg^{2+} interaction site (see Supplemental Figure 3 online). Although the Gly_6 NH peak of Mg^{2+}-CaM4 EF-hand II is not observed in ^1H-^{15}N shift correlation spectra, signals corresponding to other main chain NH groups of the EF-loop are present, and the loss of this peak likely reflects a weaker Mg^{2+} affinity at this site than EF-hand I (Huang et al., 2010). Interestingly, these results with plant CaMs differ from that seen with m-CaM in which again all four EF-hands bind Mg^{2+}, but EF-hands I and IV do so with the strongest affinity (Ohki et al., 1997).

The preference of Mg^{2+} for the EF-hands of the N-terminal lobes of CaM1 and CaM4 as well as the localized binding of this cation to the EF-loops is supported by studies using the paramagnetic manganese cation (Mn^{2+}). Mn^{2+} has an ionic radius close to that of Mg^{2+} (0.67 Å versus 0.72 Å, respectively, compared with 1.06 Å for Ca^{2+}; Senguen and Grabarek, 2012), and both ions favor six ligands arranged in an octahedral geometry, but the unpaired nature of the nuclear spins in this cation cause the broadening/loss of nearby NMR signals (Aravind et al., 2008). At low Mn^{2+} concentrations and in the presence of Ca^{2+} and Mg^{2+}, the N-terminal Gly_6 NH peaks of Ca^{2+}-bound CaM1 or CaM4 are observed to broaden and disappear first, indicating a ready interaction with these EF-hands (Figure 4). By contrast, no observable changes were seen for Gly-98 and Gly-134 of EF-hands III and IV at this low concentration. As the amount of Mn^{2+} is increased, the Gly-134 peak of both CaM1 and CaM4 is seen to broaden, while little change is observed for Gly-98, even at higher Mn^{2+} concentrations. This observation suggests that Mg^{2+} binds EF-III of both isoforms with the weakest affinity. In addition to showing the direct influence of the paramagnetic ion on the NMR signal of critical residues of the EF-loop, attributable to the presence of Ca^{2+}, this competition experiment is also indicative of the relative Ca^{2+} binding strength of the various EF-loops. For both CaM1 and CaM4, Mn^{2+} appears to have the greatest affinity for EF-hand II, contrasting with Mg^{2+}, which, as our results above suggest, binds the most strongly to EF-hand I. This discrepancy could be explained by the greater affinity of EF-hand I for Ca^{2+} compared with EF-hand II. Because of this increased Ca^{2+} affinity, Mn^{2+} likely cannot readily compete the Ca^{2+} off and binds EF-hand II first.

Table 2. Thermodynamic Parameters for the Binding of Ca^{2+} to CaM1 or CaM4

	No Mg^{2+}			+ 10 mM Mg^{2+}		
CaM	ΔH (kJ mol^{-1})[a]	$-T\Delta S$ (kJ mol^{-1})	ΔS (J K^{-1} mol^{-1})[b]	ΔH (kJ mol^{-1})	$-T\Delta S$ (kJ mol^{-1})	ΔS (J K^{-1} mol^{-1})
s-CaM1						
Site 1	5.6 ± 0.1	−36.7 ± 0.1	121.1 ± 0.3	−14.7 ± 0.2	−14.3 ± 0.4	47.1 ± 1.4
Site 2	9.8 ± 1.0	−39.1 ± 1.1	129.2 ± 3.5	−12.5 ± 0.1	−14.6 ± 0.0	48.3 ± 0.1
Site 3	−11.0 ± 0.3	−17.5 ± 0.2	57.9 ± 0.7	4.9 ± 1.2	−26.5 ± 1.2	87.3 ± 4.0
Site 4	0.5 ± 0.5	−23.7 ± 0.7	78.2 ± 2.2	−11.8 ± 0.8	−12.6 ± 0.6	41.7 ± 2.1
s-CaM4						
Site 1	−101.6 ± 36.4	72.8 ± 36.8	−240.2 ± 121.6	−49.8 ± 3.3	22.9 ± 3.9	−75.6 ± 12.8
Site 2	70.3 ± 35.5	−107.8 ± 37.1	355.9 ± 122.5	−66.7 ± 7.1	41.5 ± 7.0	−137.1 ± 23.0
Site 3	124.3 ± 55.0	−148.9 ± 53.5	491.3 ± 176.5	110.8 ± 2.7	−135.7 ± 2.6	447.7 ± 8.7
Site 4	−182.0 ± 55.4	149.7 ± 54.6	−494.0 ± 180.2	−65.6 ± 4.7	37.6 ± 4.9	−124.0 ± 16.0

From our NMR data, sites 1 and 2 can be assigned to the C-terminal lobe and sites 3 and 4 to the N-terminal lobe.
[a] $\Delta H = \Delta H_{bind} + \Delta H_{conf}$, where $\Delta H_{bind} = 0$.
[b] $\Delta S = \Delta S_{bind} + \Delta S_{conf}$, where $\Delta S_{bind} = 90.6$ J K^{-1} mol^{-1} (see text for details).

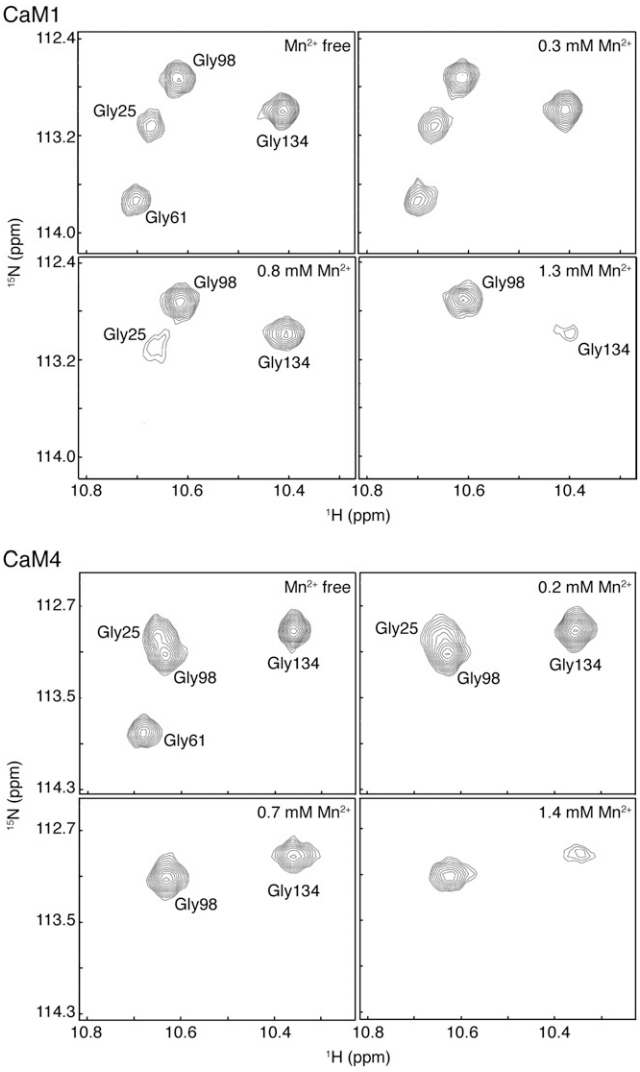

Figure 4. Paramagnetic Effects of Mn^{2+} on the Ca^{2+}-Bound Spectra of CaM1 or CaM4.

Selected regions of [^{15}N-^{1}H]-HSQC spectra recorded during the Mn^{2+} titration of ^{15}N-labeled CaM1 or CaM4 showing Gly-25, Gly-61, Gly-98, and Gly-134 main-chain NH peaks at different Mn^{2+} concentrations. For these titrations, 509 and 706 μM CaM1 and CaM4, respectively, were used.

Mg^{2+} Stabilizes the Closed Conformation of CaM1 and CaM4

Ca^{2+} titration of Mg^{2+}-bound CaM1 or CaM4 leads to the gradual disappearance of the Mg^{2+}-associated peaks in ^{1}H-^{15}N shift correlation spectra and the concomitant appearance of those belonging to Ca^{2+}-bound CaM1 or CaM4 (Figures 2B and C). This suggests both isoforms attain the same conformation after binding Ca^{2+} in the presence and absence of Mg^{2+}, an observation predicated by the enthalpy-entropy compensation observed for Ca^{2+} binding to these isoforms under varying concentrations of Mg^{2+} (Figure 3B). Structural changes induced by the Mg^{2+} to Ca^{2+} transition can be probed by comparing the main chain ^{1}H- and ^{15}N-NMR chemical shifts of Mg^{2+}- and Ca^{2+}-bound CaM1 or CaM4 (see Supplemental Figure 2A online). In the presence of Mg^{2+}, Ca^{2+} binding to the domains of both isoforms leads to drastic changes in helix orientation and EF-loop conformation, protein structural rearrangements manifested in main chain NH chemical shift perturbations (CSPs) of a magnitude much larger than that seen on average for the Ca^{2+}-CaM:protein target interaction (Gifford et al., 2012). For both isoforms, the largest CSPs are observed to occur in the EF-loops, particularly in the loops' N-terminal (Asp-20 [+*X*], Lys-21/Ala-57) and hinge regions (Ile-27, Thr-28/Ser-101 [−*X*]). Upon Ca^{2+} chelation, both of these regions play key roles in the induced closed-to-open conformational change (see Supplemental Figure 2B online; Grabarek, 2011). Differences here indicate an altered accommodation by the EF-loop ligands for the smaller Mg^{2+} and suggest that in the presence of this cation the EF-hands remain closed. The inability of Mg^{2+} to open the EF-hands of soybean CaM1 or CaM4 is analogous to that seen with Mg^{2+}-bound m-CaM and S100G (a member of the S100 family of EF-hand proteins) (Andersson et al., 1997; Senguen and Grabarek, 2012), and is supported by previous structural work on the Mg^{2+}-bound N-terminal domain of s-CaM4 [Supplemental Figure 2B online; (Huang et al., 2010)].

The stabilization of the "closed" state of all CaM1 and CaM4 EF-hands when bound to Mg^{2+} was further confirmed by fluorescence spectroscopy studies using the hydrophobic fluorophore ANS. ANS fluorescence is strongly dependent on the local environment and is significantly weaker in water where it occurs with a maximum wavelength of 515 nm (see Supplemental Figure 2C online). Because of the similarities with its fluorescence spectrum in water, we can conclude that neither apo- nor Mg^{2+}-bound CaM1 or CaM4 interact significantly with ANS. By contrast, in the presence of Ca^{2+} and either isoform, the emission spectrum of ANS is marked by a considerable enhancement in the associated fluorescence and a blue shift of 37 nm. Both effects point to the exposure of large target binding hydrophobic pockets in this state, corroborated by the solution structures of both isoforms in the presence Ca^{2+} (Ishida et al., 2008). Taken together, our NMR and fluorescence spectroscopy data imply that although Mg^{2+} binds the Ca^{2+} binding EF-loops of CaM1 and CaM4, it does not mimic Ca^{2+}, and these EF-hands remain functionally specific for the latter cation.

Mg^{2+} Acts as a Competitive Antagonist of Ca^{2+} Binding to the EF-Hands of CaM1 and as a Competitive Antagonist and Allosteric Activator of CaM4

As would be expected for a cation that competes with Ca^{2+} for the EF-loops, in many EF-hand proteins, the influence of Mg^{2+} often manifests itself as a decrease in the measured Ca^{2+} affinity through inhibitory effects on the kinetic on-rate of Ca^{2+} binding as Ca^{2+} association becomes dependent on Mg^{2+} dissociation (see Equation 3 in Methods; Trigo-Gonzalez et al., 1992; Ohki et al., 1997; Malmendal et al., 1999). Correspondingly, Ca^{2+} titrations of Mg^{2+}-CaM1 or Mg^{2+}-CaM4 monitored via ^{1}H-^{15}N shift correlation spectra point to higher concentrations of Ca^{2+} as being required

for EF-hand saturation in the presence of 30 mM Mg^{2+} (Figure 2B). This result is particularly apparent for the N-terminal EF-hands of both isoforms, where at Ca^{2+}:protein ratios at which saturation is observed in the absence of Mg^{2+}, the Gly_6 NMR signals have yet to approximate their Ca^{2+}-bound chemical shift. Significantly higher Ca^{2+} concentrations are required to produce the Ca^{2+}-bound chemical shift and intensity of the N-terminal Gly_6 NH peaks, an unsurprising outcome as our titrations with Mn^{2+} and Mg^{2+} as well as CSP data point to the higher affinity Mg^{2+} binding sites as being located in this domain of both isoforms (Figure 4; see Supplemental Figure 2A online). Of note, despite Mg^{2+}'s apparent effects on Ca^{2+} affinity, the Ca^{2+} binding preference of the EF-hands of both isoforms remains unchanged: the C-terminal sites are occupied before the those in the N terminus.

The influence of Mg^{2+} on the Ca^{2+} affinities of CaM1 and CaM4 was investigated using ITC (Figure 3A), and the Ca^{2+} dissociation constants in the presence of 10 mM Mg^{2+} are presented in Supplemental Table 1 online. The presence of Mg^{2+} decreases the overall Ca^{2+} affinity of both isoforms by 2.7- and 6.3-fold for CaM1 and CaM4, respectively (Table 1), and unfavorable changes in respective total free energy changes [$\Delta\Delta G_{Ca(Mg)1,2,3,4}$] of 10.1 and 18.4 kJ mol^{-1} were observed under these conditions. On a domain-by-domain basis, the EF-hands of CaM1's N-terminal lobe are more affected than those of the C-terminal lobe [$\Delta\Delta G_{Ca(Mg)N}$ = 5.7 kJ mol^{-1} versus $\Delta\Delta G_{Ca(Mg)C}$ = 4.3 kJ mol^{-1}]. By contrast, the C-terminal EF-hands of CaM4 are more affected than those of the N-terminal domain [$\Delta\Delta G_{Ca(Mg)N}$ = 4.1 kJ mol^{-1} versus $\Delta\Delta G_{Ca(Mg)C}$ = 14.3 kJ mol^{-1}], an unexpected finding as our NMR data point to the EF-hands of the N-terminal domain as containing the higher affinity Mg^{2+} binding sites for both isoforms (Figures 2B and 4; see Supplemental Figures 1 and 2A online). This discrepancy suggests Mg^{2+} acts not only as a competitive antagonist to Ca^{2+} binding to the N-terminal EF-hands of CaM4 but that it also serves as an allosteric activator, increasing the observed Ca^{2+} affinity of these EF-hands by folding the domain and thus paying the entropic cost in conformational energy of cation binding. As a result, the increased intrinsic Ca^{2+} affinity of the folded EF-hand pair in the presence of Mg^{2+} masks the competitive effect of the smaller cation and the $\Delta\Delta G_{Ca(Mg)}$ for Ca^{2+} binding to this domain in the absence and presence of Mg^{2+} is less than would be expected.

Also apparent from the presented ITC data is the effect of $MgCl_2$ on the thermodynamic driving factors of Ca^{2+} binding to CaM1 and CaM4 (Figure 3A). Upon analysis, the much simpler and predominantly exothermic isotherms for Ca^{2+} binding to either isoform reflect the favorable ΔH_{conf} that accompanies the binding of this cation to all but one EF-hand of CaM1 and CaM4 (Table 2). For CaM1, this process is accompanied by unfavorable changes in conformational entropy for all four EF-hands (ΔS_{conf} values of −43.5, −42.3, −3.3, and −48.0 J K^{-1} mol^{-1} for the Ca^{2+} binding sites in order of affinity, respectively). Both trends can be explained by the conformational instability of Mg^{2+}-bound CaM1 (see Supplemental Figure 2A online). The binding of Ca^{2+} first to the C-terminal and then the N-terminal EF-loops would stabilize the isoform's conformation, leading to the formation of energetically favorable contacts (and, thus, a negative ΔH_{conf}) but also the rigidification of CaM1 and the accompanying unfavorable changes in ΔS_{conf}. Similarly, the interaction of Ca^{2+} with Mg^{2+}-CaM4 is characterized by favorable changes in enthalpy and overall unfavorable changes in entropy for all but one EF-hand. As evidenced by the missing peaks in NMR spectra, the conformational instability of the C-terminal lobe of Mg^{2+}-CaM4 is greater than that of Mg^{2+}-CaM1 (see Supplemental Figure 2A online), and as a result, the adverse loss of molecular flexibility is higher, and unfavorable changes in conformational entropy (ΔS_{conf} = −166.2, −227.7, 357.1, and −214.6 J K^{-1} mol^{-1}, for the bindings sites, respectively) eclipse the favorable entropy of Ca^{2+} desolvation (90.6 J K^{-1} mol^{-1}; see above). For both isoforms, one Ca^{2+} binding site remains enthalpically unfavorable and entropically favorable: site 3. From these characteristics, the identify of this site is likely EF-hand I as, in the presence of Mg^{2+}, this site is well formed and structurally stable.

Competition from Free Mg^{2+} Affects the Activating Ca^{2+} Concentration of CaM1 and CaM4

Unlike Ca^{2+}, the binding of Mg^{2+} to these proteins is accompanied by a monophasic endothermic reaction (CaM1) or limited heat release (CaM4), hindering direct measurement of the Mg^{2+} binding affinities. However, as Mg^{2+} acts as a competitive antagonist of the Ca^{2+} binding EF-loops, the mean value of the Mg^{2+} dissociation constants, $K_{d,Mg,mean}$, can be determined from the effect this cation has on the measured Ca^{2+} dissociation constants (see Equation 5 in Methods). Calculated $K_{d,Mg,mean}$ values of 6.3 and 2.0 mM for s-CaM1 and s-CaM4, respectively, agree with that previously determined for the N-terminal lobe of m-CaM (Malmendal et al., 1999) but are significantly lower than that reported for other EF-hand-containing proteins for which Mg^{2+} affinities as high as 10^{-6} M have been measured (Aravind et al., 2008). Under stress Mg^{2+} concentrations (1 mM Mg^{2+}), competition from this cation decreases the $K_{d,Ca,mean,app}$ by a factor of 1.2 and 1.7 for soybean CaM1 and CaM4, respectively. As a consequence, Mg^{2+} effectively lowers the population of the Ca^{2+} loaded state of CaM4 by a factor of 1.4 to 3.0 over the entire range of global cytosolic Ca^{2+} conditions (Figure 5A). By contrast, as a result of its increased selectivity for Ca^{2+}, the drop in saturation for CaM1 is only a factor of 1.1 to 1.2. The effects of Mg^{2+} competition are most prominent for the C-terminal domain of CaM4, where the presence of this cation reduces the population of the Ca^{2+}-loaded state by a factor of 1.5 to 3.7. In the absence of a CaM-binding domain that can modulate the observed Ca^{2+} affinity (Peersen et al., 1997; Gifford et al., 2007), under these conditions, no more than 40% of CaM1 or 50% of CaM4 molecules are ever saturated with Ca^{2+}. The colocalization of CaM1 or CaM4 near a plasma membrane or organelle Ca^{2+} release channel could also increase the degree of saturation in either isoform as, due to the slow diffusion rate of this metal cation, the Ca^{2+} concentration in these microdomains can be orders of magnitude higher than that measured globally in the cytoplasm (Grant et al., 2000; Monshausen, 2012; Steinhorst and Kudla, 2013).

The Ca^{2+} Affinities and Selectivities of CaM1 and CaM4 Are Tuned to Their Physiological Roles

Although all CaM isoforms are ubiquitously expressed in various plant tissues and show similar subcellular localization (Lee et al., 1995, 1999), cellular levels of CaM4 are much lower than that of

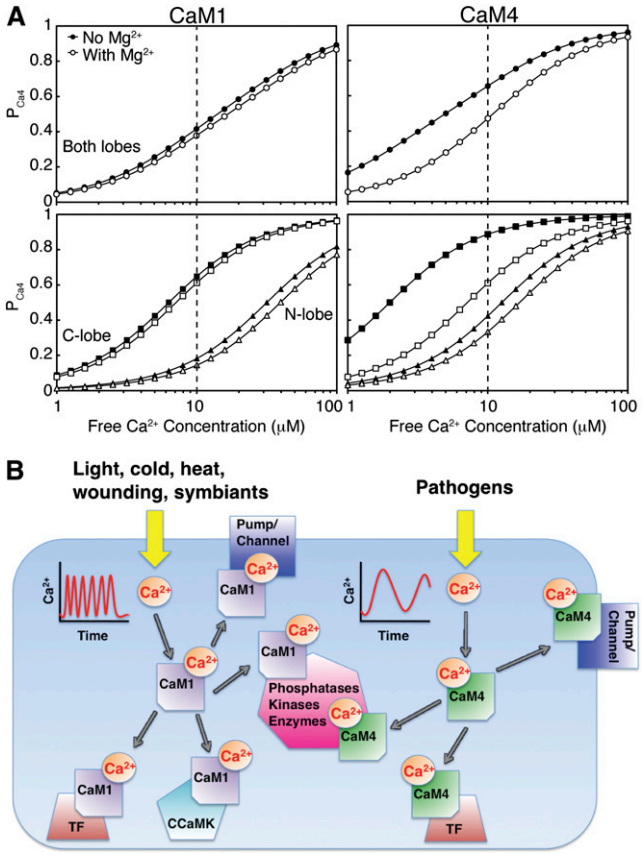

Figure 5. Ca^{2+} Affinities and Selectivities of CaM1 and CaM4 Are Tuned to Their Physiological Roles.

(A) Populations of Ca^{2+}-loaded CaM1 and CaM4 as a function of free [Ca^{2+}] in the absence and presence of 1 mM Mg^{2+}. The curves were calculated using the Adair equation: $P_{Ca2} = \frac{K_1[Ca^{2+}]+2K_1K_2[Ca^{2+}]^2}{2(1+K_1[Ca^{2+}]+K_1K_2[Ca^{2+}]^2)}$ and $P_{Ca4} = \frac{P^N_{Ca2}+P^C_{Ca2}}{2}$. Dashed line represents the upper limit of the global concentration of cytosolic free Ca^{2+}.

(B) Schematic representing the extracellular stimulants, approximate Ca^{2+} signature, and different intermolecular interactions of CaM1 and CaM4. TF, transcription factor; CCaMK, Ca^{2+}- and Ca^{2+}-CaM–dependent protein kinase.

CaM1 and, instead, rapidly and dramatically rise in specific response to pathogen elicitors or salt stress (Heo et al., 1999; Park et al., 2004b). By contrast, the same treatments have no effect on CaM1 expression levels. The role of CaM4 as a central component of plant host-defense pathways is beginning to emerge, and several target–protein interactions have been identified (Figure 5B) (Kondo et al., 1999; Park et al., 2004a; Alkharouf et al., 2006; Boursiac et al., 2010; Spalding and Harper, 2011). Ca^{2+} influx into the cytosol and nucleoplasm is an early plant cell response to pathogen attack, serving as a messenger to regulate specific downstream defense pathways (Ma et al., 2008; Reddy et al., 2011). In plant cells, although an increase in cytoplasmic Ca^{2+} concentration is an indicator of a wide variety of stimuli, each stimulus is accompanied by a Ca^{2+} signal of characteristic amplitude, duration, and oscillation frequency that is subsequently interpreted by Ca^{2+} binding proteins (McAinsh and Pittman, 2009; Batistič and Kudla, 2012). The sustained level of cytosolic/nuclear Ca^{2+} evoked by pathogen effectors differs considerably from the repetitive oscillation patterns seen during abiotic stresses or host–symbiant interactions (Lecourieux et al., 2002; Moscatiello et al., 2006; Dodd et al., 2010). During avirulent interactions, this continuous wave of Ca^{2+} is key to the induction of host-defense genes, one of which is *CaM4*, as well as the subsequent hypersensitive resistance response, the process of localized programmed cell death used to stop pathogen spread at a site of infection (Grant et al., 2000; Thuleau et al., 2013).

Our analysis suggests the differing sensitivities of CaM1 and CaM4 to both Ca^{2+} and Mg^{2+} would help to fine-tune each isoform to activate its required protein targets. Due to the constitutive high expression levels of *CaM1/3*, it is likely this isoform responds to the individualized, fast, spiking signals characteristic of abiotic stresses or root nodule host-symbiant relationships (McAinsh and Pittman, 2009; Wu and Jinn, 2012). Competition from Mg^{2+} does not significantly affect Ca^{2+} binding to CaM1, enabling this isoform to rapidly respond to the Ca^{2+} signal. By contrast, the reduced selectivity of CaM4 for the Mg^{2+} cation and the resulting Mg^{2+}/Ca^{2+} competition would slow the response of this isoform to an increased cytoplasmic Ca^{2+} concentration as the association of Ca^{2+} is now dependent on Mg^{2+} dissociation (see Equation 3 in Methods). The effect of this Mg^{2+}/Ca^{2+} competition on the responsiveness of CaM4 was observed previously in CaM-target enzyme activation assays. In $MgCl_2$-containing experiments comparing the Ca^{2+}-dependent activation ability of CaM1 and CaM4 on representative CaM-dependent enzymes (phosphodiesterase, CaM-dependent kinase II, or smooth muscle myosin light chain kinase), CaM4 displayed a reduced sensitivity to Ca^{2+}, and, thus, activation ability, despite binding these same protein targets with a similar intermolecular affinity as CaM1 (Lee et al., 2000; Van Lierop et al., 2002; Yamniuk and Vogel, 2005), and Ca^{2+} with a higher affinity, as presented here. As a result of the influence of Mg^{2+}, the energetics of Ca^{2+}'s interaction with CaM4 are more favorable to the sustained increase in cytosolic Ca^{2+} concentration that accompanies host–pathogen interaction, and the higher Ca^{2+} affinity of CaM4 would mean it would successfully compete with CaM1 for the Ca^{2+} signal under these conditions, ensuring the CaM–target protein interactions required for pathogen resistance get precedence. The plant nitric oxide synthase (NOS) could be regulated in such a manner. Along with an elevated cytoplasmic Ca^{2+} concentration, the free radical nitric oxide is known to play a role in plant defense and the hypersensitive resistance response (Ma et al., 2008). The activation of animal NOS is Ca^{2+}-CaM dependent, and biochemical and genetic evidence points to a similar regulatory mechanism for the plant enzyme (Ma et al., 2008). Plant NOS, recently identified and characterized in the green alga *Ostreococcus tauri*, is 45% similar to animal NOS and includes a CaM binding domain (Foresi et al., 2010). Both isoforms of soybean CaM bind animal NOS with equal strength, but this CaM-dependent enzyme is inhibited by s-CaM1 and activated by s-CaM4 (Cho et al., 1998; Yamniuk and Vogel, 2005). The hindering effects of a Mg^{2+}/Ca^{2+} competition on the responsiveness of s-CaM4 would further tune the activation of NOS to be timed with the appropriate Ca^{2+} signal; in the absence of the sustained elevated cytoplasmic Ca^{2+} concentration that accompanies pathogen attack, the effects of this cation competition on

CaM4 would facilitate CaM1 binding NOS, thus preventing enzyme activation.

In conclusion, we characterized the Ca^{2+} and Mg^{2+} binding abilities of two plant CaM isoforms: one representing a conserved CaM (s-CaM1) and one a divergent isoform (s-CaM4). Although determined in vitro, these binding constants represent the intrinsic Ca^{2+} affinities of these isoforms and thus are physiologically important. Our results suggest that in addition to having differential target regulation abilities, the different CaMs also have unique affinities for the activating Ca^{2+} cation. That these proteins would have differing affinities would not be readily predicted from their primary amino acid sequences. A high degree of identity/similarity exists between the CaMs of different plant species, and our findings can likely be extended to close homologs of soybean CaM1: s-CaM2 (alfalfa CaM, barley CaM, and At-CaM1/2/6/7) and s-CaM4 (s-CaM5, At-CML8, and antigens present in Chinese cabbage [*Brassica rapa chinensis*], rice [*Oryza sativa*], and tobacco [*Nicotiana tabacum*]) (Lee et al., 1995; Zielinski, 2002; Park et al., 2010) (Figure 1B). Because of their sessile nature it is perhaps not surprising that Ca^{2+} signaling pathways are more sophisticated in plants, and it appears that differing responsiveness toward the Ca^{2+} signal adds to the complexity of the disparity in target activation abilities already observed for these isoforms. Our knowledge of the plant stress response, of significant application in agriculture, relies on understanding the divergent nature of the CaM isoforms.

METHODS

Sequence Alignment

Amino acid sequences for m-CaM, CaMs, and select CMLs from soybean (*Glycine max*) and *Arabidopsis thaliana* were aligned with ClustalW2 using the default alignment parameters: Gonnet protein weight matrix, gap open and extension scores of 10 and 0.2, respectively, and a gap distance score of 5 (Larkin et al., 2007).

Protein Expression and Purification

CaM1 and CaM4 from soybean were overexpressed and purified from *Escherichia coli* strain BL21 (DE3), containing the pET-3d plasmid as described previously (Ishida et al., 2008). ^{15}N-labeled or ^{13}C,^{15}N-labeled CaM1 and CaM4 were prepared in M9 media containing 0.5 g/L $^{15}NH_4Cl$ and 3 g/L of either unlabeled or ^{13}C-labeled Glc. All proteins were purified to homogeneity by Ca^{2+}-dependent phenyl-Sepharose chromatography (Ishida et al., 2008). The concentrations of CaM1 and CaM4 were determined using ε_{276} CaM1 = 1450 M^{-1} cm^{-1} and ε_{276} CaM4 = 2900 M^{-1} cm^{-1}. For the biophysical studies described here, plastic ware and glass NMR tubes were rinsed with 1 M HCl, and Chelex-100–treated buffers and ultrapure grade chemicals from Sigma-Aldrich were employed in order to minimize Ca^{2+} contamination. Exogenous Ca^{2+} was removed from CaM1 and CaM4 samples using a Calcium Sponge S column (Molecular Probes).

Fluorescence Spectroscopy

Steady state ANS binding experiments were recorded on a Varian Cary Eclipse fluorescence spectrophotometer at 25°C with an excitation wavelength of 370 nm, and the fluorescence emission was recorded from 400 to 600 nm. The excitation and emission slit widths were 5 and 5 nm or 5 and 10 nm for CaM1 and CaM4, respectively. Samples contained 120 μM ANS and 20 μM CaM1 or CaM4 in a buffer containing 20 mM HEPES, pH 7.5, 100 mM KCl, and 1 mM DTT. For all experiments, the sample volume was 1 mL.

ITC

All ITC experiments were performed on a MicroCal VP-ITC microcalorimeter: 100 μM CaM1 or CaM4 was titrated with 5.1 mM $CaCl_2$ in 20 mM HEPES, pH 7.5, 1 mM *tris*(2-carboxyethyl)phosphine, and either 100 mM KCl with 0, 0.5, or 2 mM $MgCl_2$, 70 mM KCl with 10 mM $MgCl_2$, or 10 mM KCl with 30 mM $MgCl_2$. Prior to each experiment, the ITC sample cell was soaked with 10% EDTA to remove contaminating Ca^{2+} and subsequently washed extensively with Ca^{2+}-free buffer. Data were fitted using the four sequential sites model in the MicroCal Origin software to determine the binding constant (K) and the ΔH associated with binding. The ΔH and K values were then used to calculate the ΔS through the following relationships:

$$\Delta G = -RT \ln K \quad (1)$$

$$\Delta G = \Delta H\text{-}T\Delta S \quad (2)$$

The fitted K values are influenced by the kinetic on- (k_{on}) and off-rate (k_{off}) of Ca^{2+} binding through the relationship:

$$K = \frac{k_{on}}{k_{off}} \quad (3)$$

and were converted to K_d values using:

$$K_d = \frac{1}{K} \quad (4)$$

The reported values represent the average and SE of three independent titrations performed at 30°C. The strength of Mg^{2+} binding ($K_{d,Mg,mean}$) can be estimated from the effect of Mg^{2+} on the observed Ca^{2+} binding constants ($K_{Ca,mean,app}$ at 10 mM $MgCl_2$ versus $K_{Ca,mean}$ at 0 mM $MgCl_2$) using an equation describing the competition of two ions for a single site (Bryant, 1985):

$$K_{d,Mg,mean} = \frac{K_{Ca,mean,app}[Mg^{2+}]}{K_{Ca,mean} - K_{Ca,mean,app}} \quad (5)$$

where $K_{Ca,mean,app} = [(K_{Ca1}K_{Ca2}K_{Ca3}K_{Ca4})_{app}]^{1/4}$ and $K_{Ca,mean} = (K_{Ca1}K_{Ca2}K_{Ca3}K_{Ca4})^{1/4}$

NMR Spectroscopy

All NMR experiments were performed on a Bruker Avance 500 MHz spectrometer equipped with a triple resonance inverse cryogenic probe. Main-chain NMR signal assignment of Mg^{2+}-bound CaM1 was completed with two-dimensional [^{15}N-^{1}H]-HSQC and three-dimensional HNCACB, CBCA-CONH, HNCACO, and HNCO experiments using ~0.5 mM ^{13}C,^{15}N-labeled CaM1, 100 mM KCl, 30 mM $MgCl_2$, 10 mM DTT, and 0.5 mM 2,2-dimethyl-2-silapentane-5-sulfonate (DSS) in 90% water/10% ^2H_2O), pH 6.8. The main-chain NMR signal assignments of Mg^{2+}-CaM4, Ca^{2+}-CaM1, and Ca^{2+}-CaM4 were obtained from previous publications in which they were acquired under similar conditions (Ishida et al., 2008; Huang et al., 2010).

Ca^{2+} and Mg^{2+} titrations were performed with 40.4 and 40.6 mM stocks of $CaCl_2$ and $MgCl_2$, respectively. The protein concentration was ~0.3 mM ^{15}N-labeled CaM1 or CaM4 in 20 mM HEPES, pH 7.5, 100 mM KCl, 1 mM DTT, 90% water/10% ^2H_2O, and either 0 or 30 mM $MgCl_2$. For each titration, an aliquot of the stock solution was added to the NMR tube containing the protein solution and mixed, and a two-dimensional [^{15}N-^{1}H]-selective optimized-flip-angle short-transient heteronuclear multiple quantum coherence experiment was recorded at 30°C (Schanda et al., 2005). The total experimental time for each spectrum was 3 min. [^{15}N-^{1}H]-HSQC spectra of apo-, Mg^{2+}-, and Ca^{2+}-bound CaM1 or CaM4 (both in the presence and absence of 30 mM $MgCl_2$) were also acquired.

Mn^{2+} titrations were performed with ~0.5 mM Ca^{2+}-bound CaM1 or ~0.7 mM CaM4 in 20 mM HEPES, pH 7.5, 100 mM KCl, 30 mM $MgCl_2$, 5 mM DTT, 90% water/10% ^2H_2O, and 0.5 mM DSS, with a 16-fold molar excess of $CaCl_2$. Mn^{2+} was titrated into the sample from a 100 mM $MnCl_2$ stock solution. The titrations were performed at 30°C and monitored using [^{15}N-^{1}H]-HSQC spectra. No titration was performed beyond a Mn^{2+}: protein ratio of 2 when the water peak started showing broadening due to the paramagnetic Mn^{2+} (Aravind et al., 2008).

Chemical shifts in the assignment spectra were referenced using DSS to obtain the ^{1}H, ^{15}N, and ^{13}C chemical shifts. All spectra were processed using the program NMRPipe (Delaglio et al., 1995) and analyzed using the NMRView software (Johnson and Blevins, 1994). CSPs in the [^{15}N-^{1}H]-HSQC spectra of Ca^{2+}- and Mg^{2+}-bound CaM1 or CaM4 were calculated as the weighted averaged chemical shift difference of the ^{1}H and ^{15}N resonances according to the equation (Grzesiek et al., 1996):

$$\mathrm{CSP} = \sqrt{(\Delta H_N)^2 + (\Delta N/5)^2} \quad (6)$$

Accession Numbers

Sequence data from this article can be found in the GenBank/EMBL libraries under the following accession numbers: s-CaM1 (NP_001238237.1), s-CaM4 (AAA341015.1), and m-CaM (AAD45181.1). The accession numbers for the amino acid sequences used in the sequence alignment can be found in Supplemental Table 2 online.

Supplemental Data

The following materials are available in the online version of this article.

Supplemental Figure 1. [^{15}N-^{1}H]-HSQC Spectra of Ca^{2+}-Bound, Mg^{2+}-Bound, or Apo-^{15}N-Labeled CaM1 or CaM4 with the Assigned EF-Hand Gly_6 Peaks Indicated.

Supplemental Figure 2. Conformational Changes Induced upon Binding of Ca^{2+}- to Mg^{2+}-CaM1 or Mg^{2+}-CaM4.

Supplemental Figure 3. Overlay of [^{15}N-^{1}H]-HSQC Spectra Monitoring the Mg^{2+} Titration of 0.2 mM ^{15}N-Labeled CaM1.

Supplemental Table 1. Individual Dissociation Constants for Ca^{2+} Binding to CaM1 or CaM4 in the Absence and Presence of Mg^{2+}.

Supplemental Table 2. Protein Names and IDs Used for the Sequence Alignment.

Supplemental References 1. References for Supplemental Figures 1-3.

Supplemental Data Set 1. Alignments Used to Generate the Sequence Alignment in Figure 1.

ACKNOWLEDGMENTS

This research was supported by an operated grant from the Natural Sciences and Engineering Research Council of Canada. H.J.V. holds a scientist award from the Alberta Heritage Foundation for Medical Research.

AUTHOR CONTRIBUTIONS

J.L.G. designed the research, performed research, analyzed data, and wrote the article. M.J. analyzed data. J.M. performed research. H.I. contributed new analytical tools. H.J.V. designed the research and wrote the article.

Received April 26, 2013; revised October 3, 2013; accepted October 23, 2013; published November 19, 2013.

REFERENCES

Alkharouf, N.W., Klink, V.P., Chouikha, I.B., Beard, H.S., MacDonald, M.H., Meyer, S., Knap, H.T., Khan, R., and Matthews, B.F. (2006). Timecourse microarray analyses reveal global changes in gene expression of susceptible *Glycine max* (soybean) roots during infection by *Heterodera glycines* (soybean cyst nematode). Planta **224:** 838–852.

Andersson, M., Malmendal, A., Linse, S., Ivarsson, I., Forsén, S., and Svensson, L.A. (1997). Structural basis for the negative allostery between Ca(2+)- and Mg(2+)-binding in the intracellular Ca(2+)-receptor calbindin D9k. Protein Sci. **6:** 1139–1147.

Aravind, P., Chandra, K., Reddy, P.P., Jeromin, A., Chary, K.V., and Sharma, Y. (2008). Regulatory and structural EF-hand motifs of neuronal calcium sensor-1: Mg^{2+} modulates Ca^{2+} binding, Ca^{2+}-induced conformational changes, and equilibrium unfolding transitions. J. Mol. Biol. **376:** 1100–1115.

Batistič, O., and Kudla, J. (2012). Analysis of calcium signaling pathways in plants. Biochim. Biophys. Acta **1820:** 1283–1293.

Bouché, N., Yellin, A., Snedden, W.A., and Fromm, H. (2005). Plant-specific calmodulin-binding proteins. Annu. Rev. Plant Biol. **56:** 435–466.

Boursiac, Y., Lee, S.M., Romanowsky, S., Blank, R., Sladek, C., Chung, W.S., and Harper, J.F. (2010). Disruption of the vacuolar calcium-ATPases in Arabidopsis results in the activation of a salicylic acid-dependent programmed cell death pathway. Plant Physiol. **154:** 1158–1171.

Bryant, D.T. (1985). Quin 2: The dissociation constants of its Ca^{2+} and Mg^{2+} complexes and its use in a fluorimetric method for determining the dissociation of Ca^{2+}-protein complexes. Biochem. J. **226:** 613–616.

Cho, M.J., Vaghy, P.L., Kondo, R., Lee, S.H., Davis, J.P., Rehl, R., Heo, W.D., and Johnson, J.D. (1998). Reciprocal regulation of mammalian nitric oxide synthase and calcineurin by plant calmodulin isoforms. Biochemistry **37:** 15593–15597.

Choi, J.Y., et al. (2002). Identification of calmodulin isoform-specific binding peptides from a phage-displayed random 22-mer peptide library. J. Biol. Chem. **277:** 21630–21638.

Dagher, R., Peng, S., Gioria, S., Fève, M., Zeniou, M., Zimmermann, M., Pigault, C., Haiech, J., and Kilhoffer, M.C. (2011). A general strategy to characterize calmodulin-calcium complexes involved in CaM-target recognition: DAPK and EGFR calmodulin binding domains interact with different calmodulin-calcium complexes. Biochim. Biophys. Acta **1813:** 1059–1067.

Delaglio, F., Grzesiek, S., Vuister, G.W., Zhu, G., Pfeifer, J., and Bax, A. (1995). NMRPipe: A multidimensional spectral processing system based on UNIX pipes. J. Biomol. NMR **6:** 277–293.

Dodd, A.N., Kudla, J., and Sanders, D. (2010). The language of calcium signaling. Annu. Rev. Plant Biol. **61:** 593–620.

Fischer, R., Koller, M., Flura, M., Mathews, S., Strehler-Page, M.A., Krebs, J., Penniston, J.T., Carafoli, E., and Strehler, E.E. (1988). Multiple divergent mRNAs code for a single human calmodulin. J. Biol. Chem. **263:** 17055–17062.

Foresi, N., Correa-Aragunde, N., Parisi, G., Caló, G., Salerno, G., and Lamattina, L. (2010). Characterization of a nitric oxide synthase from the plant kingdom: NO generation from the green alga *Ostreococcus tauri* is light irradiance and growth phase dependent. Plant Cell **22:** 3816–3830.

Gifford, J.L., Ishida, H., and Vogel, H.J. (2011). Fast methionine-based solution structure determination of calcium-calmodulin complexes. J. Biomol. NMR **50:** 71–81.

Gifford, J.L., Ishida, H., and Vogel, H.J. (2012). Structural insights into calmodulin-regulated L-selectin ectodomain shedding. J. Biol. Chem. **287:** 26513–26527.

Gifford, J.L., and Vogel, H.J. (2013). EF-hand proteins and magnesium. In Encyclopedia of Metalloproteins, R.H. Kretsinger, V.N. Uversky, and E.A. Permyakov, eds (New York: Springer), pp. 775–783.

Gifford, J.L., Walsh, M.P., and Vogel, H.J. (2007). Structures and metal-ion-binding properties of the Ca^{2+}-binding helix-loop-helix EF-hand motifs. Biochem. J. **405:** 199–221.

Gilli, R., Lafitte, D., Lopez, C., Kilhoffer, M., Makarov, A., Briand, C., and Haiech, J. (1998). Thermodynamic analysis of calcium and magnesium binding to calmodulin. Biochemistry **37:** 5450–5456.

Grabarek, Z. (2011). Insights into modulation of calcium signaling by magnesium in calmodulin, troponin C and related EF-hand proteins. Biochim. Biophys. Acta **1813:** 913–921.

Grant, M., Brown, I., Adams, S., Knight, M., Ainslie, A., and Mansfield, J. (2000). The RPM1 plant disease resistance gene facilitates a rapid and sustained increase in cytosolic calcium that is necessary for the oxidative burst and hypersensitive cell death. Plant J. **23:** 441–450.

Grunwald, E., and Steel, C. (1995). Solvent reorganization and thermodynamic enthalpy-entropy compensation. J. Am. Chem. Soc. **117:** 5687–5692.

Grzesiek, S., Bax, A., Clore, G.M., Gronenborn, A.M., Hu, J.S., Kaufman, J., Palmer, I., Stahl, S.J., and Wingfield, P.T. (1996). The solution structure of HIV-1 Nef reveals an unexpected fold and permits delineation of the binding surface for the SH3 domain of Hck tyrosine protein kinase. Nat. Struct. Biol. **3:** 340–345.

Heo, W.D., Lee, S.H., Kim, M.C., Kim, J.C., Chung, W.S., Chun, H.J., Lee, K.J., Park, C.Y., Park, H.C., Choi, J.Y., and Cho, M.J. (1999). Involvement of specific calmodulin isoforms in salicylic acid-independent activation of plant disease resistance responses. Proc. Natl. Acad. Sci. USA **96:** 766–771.

Huang, H., Ishida, H., and Vogel, H.J. (2010). The solution structure of the Mg^{2+} form of soybean calmodulin isoform 4 reveals unique features of plant calmodulins in resting cells. Protein Sci. **19:** 475–485.

Igamberdiev, A.U., and Kleczkowski, L.A. (2001). Implications of adenylate kinase-governed equilibrium of adenylates on contents of free magnesium in plant cells and compartments. Biochem. J. **360:** 225–231.

Igamberdiev, A.U., and Kleczkowski, L.A. (2011). Magnesium and cell energetics in plants under anoxia. Biochem. J. **437:** 373–379.

Ishida, H., Huang, H., Yamniuk, A.P., Takaya, Y., and Vogel, H.J. (2008). The solution structures of two soybean calmodulin isoforms provide a structural basis for their selective target activation properties. J. Biol. Chem. **283:** 14619–14628.

Johnson, B.A., and Blevins, R.A. (1994). NMR View: A computer program for the visualization and analysis of NMR data. J. Biomol. NMR **4:** 603–614.

Kondo, R., Tikunova, S.B., Cho, M.J., and Johnson, J.D. (1999). A point mutation in a plant calmodulin is responsible for its inhibition of nitric-oxide synthase. J. Biol. Chem. **274:** 36213–36218.

Lafitte, D., Capony, J.P., Grassy, G., Haiech, J., and Calas, B. (1995). Analysis of the ion binding sites of calmodulin by electrospray ionization mass spectrometry. Biochemistry **34:** 13825–13832.

Larkin, M.A., et al. (2007). Clustal W and Clustal X version 2.0. Bioinformatics **23:** 2947–2948.

Lecourieux, D., Mazars, C., Pauly, N., Ranjeva, R., and Pugin, A. (2002). Analysis and effects of cytosolic free calcium increases in response to elicitors in *Nicotiana plumbaginifolia* cells. Plant Cell **14:** 2627–2641.

Lee, S.H., Johnson, J.D., Walsh, M.P., Van Lierop, J.E., Sutherland, C., Xu, A., Snedden, W.A., Kosk-Kosicka, D., Fromm, H., Narayanan, N., and Cho, M.J. (2000). Differential regulation of Ca^{2+}/calmodulin-dependent enzymes by plant calmodulin isoforms and free Ca^{2+} concentration. Biochem. J. **350:** 299–306.

Lee, S.H., et al. (1995). Identification of a novel divergent calmodulin isoform from soybean which has differential ability to activate calmodulin-dependent enzymes. J. Biol. Chem. **270:** 21806–21812.

Lee, S.H., et al. (1999). Competitive binding of calmodulin isoforms to calmodulin-binding proteins: Implication for the function of calmodulin isoforms in plants. Biochim. Biophys. Acta **1433:** 56–67.

Linse, S., Helmersson, A., and Forsén, S. (1991). Calcium binding to calmodulin and its globular domains. J. Biol. Chem. **266:** 8050–8054.

Ma, W., Smigel, A., Tsai, Y.C., Braam, J., and Berkowitz, G.A. (2008). Innate immunity signaling: Cytosolic Ca^{2+} elevation is linked to downstream nitric oxide generation through the action of calmodulin or a calmodulin-like protein. Plant Physiol. **148:** 818–828.

Malmendal, A., Linse, S., Evenäs, J., Forsén, S., and Drakenberg, T. (1999). Battle for the EF-hands: Magnesium-calcium interference in calmodulin. Biochemistry **38:** 11844–11850.

McAinsh, M.R., and Pittman, J.K. (2009). Shaping the calcium signature. New Phytol. **181:** 275–294.

McCormack, E., Tsai, Y.C., and Braam, J. (2005). Handling calcium signaling: *Arabidopsis* CaMs and CMLs. Trends Plant Sci. **10:** 383–389.

Monshausen, G.B. (2012). Visualizing Ca(2+) signatures in plants. Curr. Opin. Plant Biol. **15:** 677–682.

Moscatiello, R., Mariani, P., Sanders, D., and Maathuis, F.J. (2006). Transcriptional analysis of calcium-dependent and calcium-independent signalling pathways induced by oligogalacturonides. J. Exp. Bot. **57:** 2847–2865.

Mukherjee, S., Mohan, P.M., and Chary, K.V. (2007). Magnesium promotes structural integrity and conformational switching action of a calcium sensor protein. Biochemistry **46:** 3835–3845.

Ohki, S., Ikura, M., and Zhang, M. (1997). Identification of Mg^{2+}-binding sites and the role of Mg^{2+} on target recognition by calmodulin. Biochemistry **36:** 4309–4316.

Park, C.Y., et al. (2004a). Pathogenesis-related gene expression by specific calmodulin isoforms is dependent on NIM1, a key regulator of systemic acquired resistance. Mol. Cells **18:** 207–213.

Park, H.C., et al. (2004b). Pathogen- and NaCl-induced expression of the SCaM-4 promoter is mediated in part by a GT-1 box that interacts with a GT-1-like transcription factor. Plant Physiol. **135:** 2150–2161.

Park, H.C., Park, C.Y., Koo, S.C., Cheong, M.S., Kim, K.E., Kim, M.C., Lim, C.O., Lee, S.Y., Yun, D.J., and Chung, W.S. (2010). AtCML8, a calmodulin-like protein, differentially activating CaM-dependent enzymes in *Arabidopsis thaliana*. Plant Cell Rep. **29:** 1297–1304.

Peersen, O.B., Madsen, T.S., and Falke, J.J. (1997). Intermolecular tuning of calmodulin by target peptides and proteins: Differential effects on Ca^{2+} binding and implications for kinase activation. Protein Sci. **6:** 794–807.

Reddy, A.S., Ali, G.S., Celesnik, H., and Day, I.S. (2011). Coping with stresses: Roles of calcium- and calcium/calmodulin-regulated gene expression. Plant Cell **23:** 2010–2032.

Schanda, P., Kupce, E., and Brutscher, B. (2005). SOFAST-HMQC experiments for recording two-dimensional heteronuclear correlation spectra of proteins within a few seconds. J. Biomol. NMR **33:** 199–211.

Senguen, F.T., and Grabarek, Z. (2012). X-ray structures of magnesium and manganese complexes with the N-terminal domain of calmodulin: Insights into the mechanism and specificity of metal ion binding to an EF-hand. Biochemistry **51:** 6182–6194.

Spalding, E.P., and Harper, J.F. (2011). The ins and outs of cellular Ca(2+) transport. Curr. Opin. Plant Biol. **14:** 715–720.

Steinhorst, L., and Kudla, J. (2013). Calcium and ROS rule the waves of signaling. Plant Physiol. **163:** 471–485.

Thuleau, P., Aldon, D., Cotelle, V., Brière, C., Ranty, B., Galaud, J.P., and Mazars, C. (2013). Relationships between calcium and sphingolipid-dependent signalling pathways during the early steps of plant-pathogen interactions. Biochim. Biophys. Acta **1833:** 1590–1594.

Trigo-Gonzalez, G., Racher, K., Burtnick, L., and Borgford, T. (1992). A comparative spectroscopic study of tryptophan probes engineered into high- and low-affinity domains of recombinant chicken troponin C. Biochemistry **31:** 7009–7015.

Van Lierop, J.E., Wilson, D.P., Davis, J.P., Tikunova, S., Sutherland, C., Walsh, M.P., and Johnson, J.D. (2002). Activation of smooth muscle myosin light chain kinase by calmodulin. Role of LYS(30) and GLY(40). J. Biol. Chem. **277:** 6550–6558.

Waters, B.M. (2011). Moving magnesium in plant cells. New Phytol. **190:** 510–513.

Wu, H.C., and Jinn, T.L. (2012). Oscillation regulation of Ca^{2+}/calmodulin and heat-stress related genes in response to heat stress in rice (*Oryza sativa* L.). Plant Signal. Behav. **7:** 1056–1057.

Yamniuk, A.P., Nguyen, L.T., Hoang, T.T., and Vogel, H.J. (2004). Metal ion binding properties and conformational states of calcium- and integrin-binding protein. Biochemistry **43:** 2558–2568.

Yamniuk, A.P., and Vogel, H.J. (2005). Structural investigation into the differential target enzyme regulation displayed by plant calmodulin isoforms. Biochemistry **44:** 3101–3111.

Yamniuk, A.P., Ishida, H., Lippert, D., and Vogel, H.J. (2009). Thermodynamic effects of noncoded and coded methionine substitutions in calmodulin. Biophys. J. **96:** 1495–1507.

Zielinski, R.E. (2002). Characterization of three new members of the *Arabidopsis thaliana* calmodulin gene family: Conserved and highly diverged members of the gene family functionally complement a yeast calmodulin null. Planta **214:** 446–455.